A single-material multi-source energy harvester, multi-functional sensor and integrated harvester-sensor system – Demonstration of concept

Yang Bai, Jaakko Palosaari, Pavel Tofel, Jari Juuti*

Dr. Y. Bai, Dr. J. Palosaari, Dr. J. Juuti
Microelectronics Research Unit, Faculty of Information Technology and Electrical Engineering, University of Oulu, FI-90014 Oulu, Finland
E-mail: yang.bai@oulu.fi

Dr. P. Tofel
CEITEC – Central European Institute of Technology, Brno University of Technology, Purkynova 123, 61200 Brno, Czech Republic
Department of Physics, Faculty of Electrical Engineering and Communication, Brno University of Technology, Technicka 10, 61600 Brno, Czech Republic

Keywords: energy harvesting, sensing, multifunctional, KNBNNO, energy-efficiency design

Abstract

Single-source energy harvesters that convert solar, thermal or kinetic energy into electricity for small-scale smart electronic devices and wireless sensor networks have been under development for decades. When an individual energy source is insufficient for the required electricity generation, multi-source energy harvesting is indicated. Current technology usually combines different individual harvesters to achieve the capability of harvesting multiple energy sources simultaneously. However, this increases the overall size of the multi-source harvester but in microelectronics miniaturization is a critical consideration. In this paper, an advanced approach is demonstrated to solve this issue. A single-material energy harvesting/sensing device is fabricated using a $(K_{0.5}Na_{0.5})NbO_3$-$Ba(Ni_{0.5}Nb_{0.5})O_{3-\Delta}$ (KNBNNO) ceramic as the sole energy conversion component. This single-material component is able simultaneously to harvest or sense solar (visible light), thermal (temperature fluctuation) and kinetic (vibration) energy sources by incorporating its photovoltaic, pyroelectric and piezoelectric effects,

respectively. The interactions between different energy conversion effects, e.g. the influence of dynamic behavior on the photovoltaic effect and AC-DC signal trade-offs, are assessed and discussed. This research is expected to stimulate energy efficient design of electronic devices by integrating both harvesting and sensing functions in the same material/component.

1. Introduction

Significant efforts are currently being made to extract the maximum energy from solar panels or from thermal (e.g. geothermal) or kinetic (e.g. wind, tidal, hydro) energy sources in order to improve green/renewable electricity production.[1] However, while one source of green energy may be used for electricity production, other co-existing or co-produced sources are frequently ignored. Typical examples are the wind energy that often co-exists with sunlight or the heat produced by the overheating of solar panels.

This issue becomes significant in the case of small-scale electronic devices and wireless sensor networks.[2] Driven by advanced electronics as well as 5G and even 6G technologies,[3] the distribution of smart electronic devices and wireless sensor networks offers safety, security, convenience and accessibility. However, the provision of suitable distributed power sources has become a major issue limiting such developments.[2]

Currently, the majority of such distributed devices use batteries as their power source. Batteries frequently need to be recharged/replaced and their use is thus unpredictably costly. Because their location may be anywhere, the labor cost, rather than the cost of the batteries themselves, will dominate,[4] especially if they are located in a remote/harsh environment. For instance, if structural health monitoring sensors are installed on a bridge built in a remote area, the cost of sending engineers for maintenance and battery changing will be at least a thousand times that of the batteries. Meanwhile, many components in batteries (e.g. lead, lithium, cadmium, mercury, acid) are toxic and hazardous to both the environment and the human body if the batteries are disposed of but not properly recycled.[5-9] Batteries can also catch fire at high

operating temperatures or under severe shock, leading to safety issues. The unexpected failure of batteries may cause interruption to services, bringing inconvenience or even insecurity in certain cases.

In order to resolve this issue, energy harvesting technology has been under rapid development for the past two decades.[2] Energy harvesters typically convert ambient energy, including solar, thermal and kinetic energy, from the environment surrounding small-scale electronic devices (e.g. wearable/biomedical devices) and wireless sensor networks (structural/environmental monitoring systems) into usable electricity.[2] Ideally, these devices and sensors should be self-powered and maintenance-free and thus be independent of problematic batteries as their power sources.[10, 11] Energy harvesting is considered the ultimate solution to these power source issues. Work on energy harvester-based self-powered sensors have been previously reported.[12-17] Recently, particular attention has been paid to smart textiles/fabrics, wearable devices and industrial sensors powered by kinetic and solar energy harvesters.[18-26] Other emerging applications such as the harvesting of waste heat from lithium ion batteries have also been investigated.[27, 28]

However, the current technology can only make use of specific types of energy. Solar cells can only convert sunlight to electricity. Similarly, thermal or kinetic energy harvesters can only work with their corresponding thermal or kinetic energy sources. These single-source, individual harvesters are not powerful enough for many applications because, in reality, a single type of ambient energy is not always available or is not sufficiently stable to be converted. For instance, one could expect to power a wearable device solely by a solar cell. However, the wearer may not stay outdoors all the time. The output power of a solar cell under indoor light is typically only about 0.04 % of that under outdoor sunlight because of the dramatically decreased input energy intensity.[29] Alternatively, one could expect to power the device by a kinetic energy harvester, but again the wearer will need to rest at some stage. With a random

input of kinetic energy the output power of a piezoelectric kinetic energy harvester can be less than 1 % of that with a stable and ideal input.[30, 31]

However, the wearer will normally be in receipt of some combination of solar, thermal (e.g. temperature change when going between outdoors and indoors) and kinetic (body movement) energy at most times of the day. Similarly, most of the aforementioned devices and sensors will be exposed to one or more of these energy sources in their working environment. These sources need to be efficiently harvested simultaneously, rather than wasted to achieve a stable output energy. It is of course possible to physically combine different energy harvesters, each responding to different energy sources, within the same structure (e.g. integrating a solar cell, a thermal harvester and a kinetic harvester), so that multiple energy sources can be harvested with the same device.[32] However, this approach can lead to a summation of the costs of the single-source harvesters' production as well as additional costs related to their integration and testing. Furthermore, space is very limited in small-scale electronics. There is rarely sufficient extra space available to add more components (i.e. the miniaturization issue).[11, 33]

On the other hand, in current battery-powered sensor systems, the batteries and the sensors are designed and fabricated separately. They are connected via interface circuits, which in turn introduce energy losses, making the use of the energy inefficient. In energy harvesting systems, because the harvesters respond to external stimuli, they can act as both power source and sensor at the same time. For instance, attempts have been made to use piezoelectric energy harvesters to harvest kinetic energy (vibration) as well as to function as structural health monitoring sensors.[34, 35] However, the harvested energy was found to be insufficient, especially when shared by the sensing function, for the data to be exported wirelessly. Without wireless connectivity an energy harvesting system loses its ultimate advantage – ubiquitous data collection.

This paper proposes a concept and reports on a device aimed at solving all the above-mentioned issues. The concept is to use a single multi-functional material as the multi-

source harvesting and/or sensing component. The material is able simultaneously to harvest visible light (sunlight) via the photovoltaic effect, temperature fluctuations via the pyroelectric effect and kinetic energy via the piezoelectric effect.[36] Such a single material is used as the sole functional component in a cantilever-shaped energy harvester. The single-material device is then able to realize multi-source energy harvesting, sensing and/or a harvesting-sensing multi-functionality. This concept is demonstrated in a practical device for the first time and is expected fundamentally to advance the working principles of current hybrid, multi-source energy harvesting and sensing systems.

2. Results and Discussions

2.1. Multi-source energy conversion material

The core functional material for multi-source energy conversion has been developed and reported in the authors' previous works.[36-38] It is a perovskite-structured ceramic material of $(K_{0.5}Na_{0.5})NbO_3$ (KNN) doped with 2 mol.% $Ba(Ni_{0.5}Nb_{0.5})O_{3-\Delta}$ (BNNO). This material is abbreviated to KNBNNO hereinafter. It combines the features of the narrow band gap semiconductors (e.g. silicon) used in conventional solar cells and those of the strong ferroelectric/piezoelectric materials widely used in pyroelectric and piezoelectric energy harvesters. The introduction of Ni^{2+}-oxygen vacancy combinations into the KNN matrix unit cells eases the charge transfer from the oxygen 2*p* states at the maximum level of the valence band to the transition-metal (Nb) 4*d* states at the minimum level of the conduction band. As a result, the band gap of the material is reduced from > 3.5 eV in the UV range (the value of the parental composition KNN) to 1.6 eV in the visible range, enabling an effective absorption of the solar spectrum.[36, 37]

Meanwhile, the minimized concentration of oxygen vacancies helps the KNBNNO to maintain its ferroelectricity and piezoelectricity at the KNN level. KNN is one of the most important lead-free ferroelectric and piezoelectric materials used to substitute the conventional

lead-containing $Pb(Zr,Ti)O_3$ (PZT)-based materials for applications of sensors and energy harvesters.[39] Therefore, the KNBNNO is a lead-free ferro-/piezo-electric candidate but with the additional benefit of being a visible-light absorber and hence the ability to function as a solar cell or optoelectronic sensor. **Table 1** summarizes the parameters of the KNBNNO ceramic related to the energy harvesting and sensing functions presented in this paper. The characterizations and their derivation methods have been presented in the authors' previous work.[36] In addition, the transverse and planar electromechanical coupling coefficients (k_{31} and k_p, respectively) as well as the transverse piezoelectric coefficient (d_{31}) were calculated from resonant and anti-resonant frequencies with corresponding impedances measured with an impedance analyzer (4294A, Agilent, USA) on samples with IEEE's standard shapes.[40] In the experimental set-up a KNBNNO ceramic patch was mounted on a stainless steel cantilever and subject to vibration, temperature fluctuation and laser radiation both individually and simultaneously. Detailed information about device fabrication, characterization methods and images of the device and characterization equipment are given in the Experimental Section.

Table 1. Summary of relevant parameters of the KNBNNO ceramic used in this paper.

Parameter	**Value**	**Unit**
Density (ρ)	4.43 ± 0.02	g cm^{-3}
Band gap	1.59 ± 0.05	eV
Resistivity	52 ± 3	GΩ cm
Remanent polarization (P_r) at 1 Hz	11.3 ± 0.5	µC cm^{-2}
Piezoelectric charge coefficient (d_{33})	90 ± 5	pC N^{-1}
Piezoelectric charge coefficient (d_{31})	48 ± 1	pC N^{-1}
Relative permittivity (ε_r) at 1 kHz, after poling	930 ± 10	-
Piezoelectric voltage coefficient (g_{33})	11.9 ± 0.8	x10^{-3} Vm N^{-1}
Piezoelectric energy harvesting figure of merit (d_{33}•g_{33})	1.2 ± 0.2	x10^{-12} m^2 N^{-1}
Electromechanical coupling coefficient (k_p)	0.24 ± 0.01	-
Electromechanical coupling coefficient (k_{31})	0.18 ± 0.01	-
Piezoelectric material energy conversion efficiency (η_{piezo}), considering only the material aspect	0.44 ± 0.01	-

Dielectric loss (tan δ) at 1 kHz, after poling	0.025 ± 0.005	-
Pyroelectric coefficient (γ)	128 ± 6	μC $m^{-2}K^{-1}$

2.2. Single input energy source

2.2.1. Piezoelectric effect

The fabricated device was first tested with separate individual energy sources. The measured output current density and power density are shown in **Figure 1**. The area and volume of the KNBNNO (rather than those of the entire device) were used for the calculations of current and power densities. In Figure 1(a) an AC (alternating current) output, the typical energy conversion behavior of piezoelectric energy harvesters or sensors, is shown when the sinusoidal vibration source was turned on. Figure 1(b) shows a close-up of one cycle of the output signal in Figure 1(a). The relative vibration measured between the fixed shaker base and the shaking part was ~15 Hz in frequency, ~12 μm in peak-to-peak amplitude and ~0.06 g in peak acceleration. The equivalent peak-to-peak amplitude of the cantilever tip was measured to be ~ 205 μm. A peak output power density of about 0.3 μW cm^{-3} was obtained.

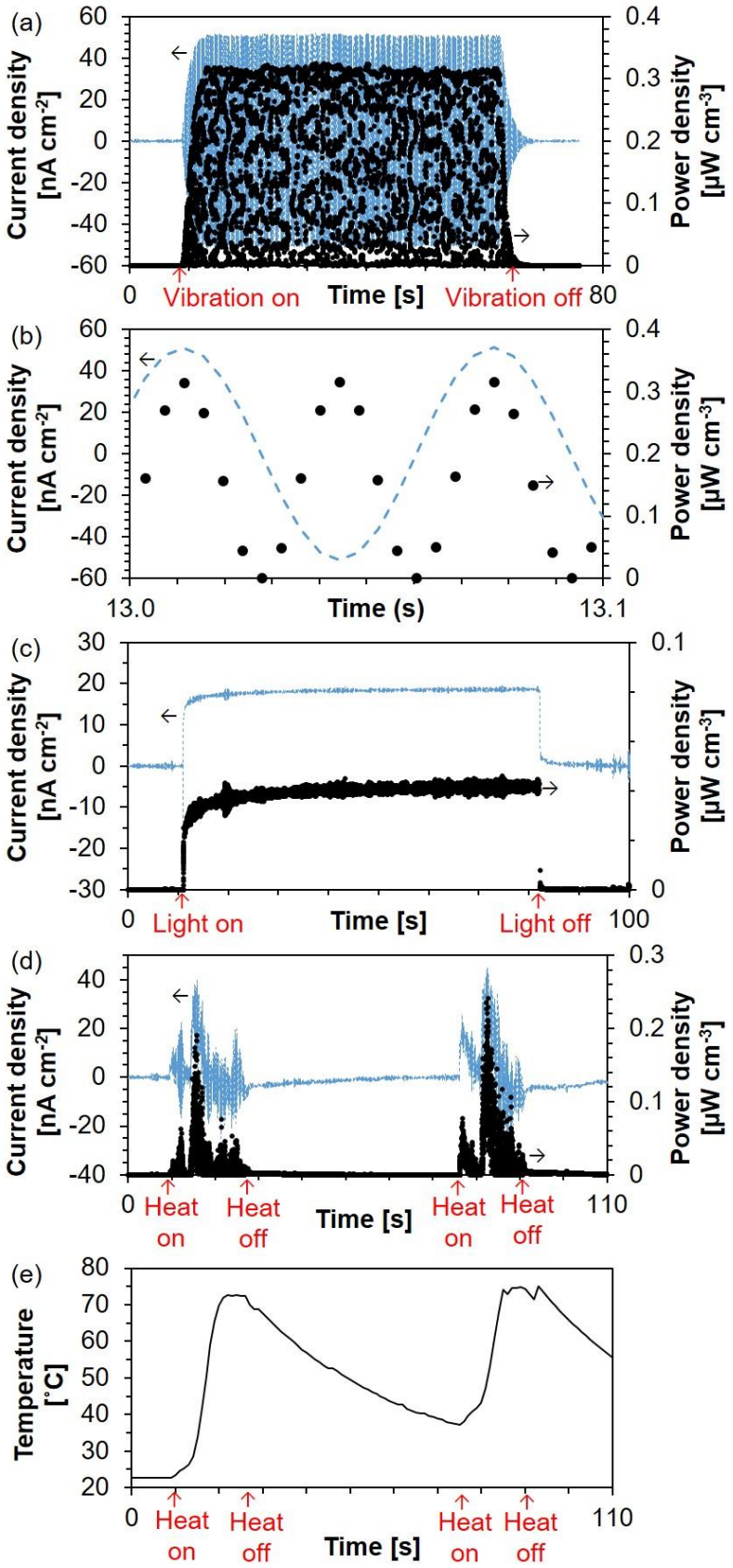

Figure 1. Output current density and power density of the KNBNNO cantilever with single input energy source: (a)(b) vibration only, (c) light only and (d) heat only. (e) Temperature profile of the measurement shown in (d).

These were not the optimized results. Previous work [31, 41-46] has shown that potential improvement can be made. Here, however, the focus was on the demonstration of the add-on effects to be gained from multi-source energy conversion. However, it can be predicted from the relevant parameters (e.g. d_{33}•g_{33}, η_{piezo}) listed in Table 1 that the optimized output power density via the piezoelectric effect of the KNBNNO energy harvester should be at a level comparable to that of a pure KNN device.[47-50] To further compare the piezoelectric performance of the KNBNNO with conventional piezoelectrics, commercial PZT-5A and PZT-5H (purchased from Piezo.com, USA, data of material properties are available from the supplier) were employed in comparison measurements.[51] Three cantilevers with the same dimensions but different materials, i.e. KNBNNO, PZT-5A and PZT-5H, respectively, were fabricated. **Figure 2** shows the spectra of the output power (RMS, root mean square) as a function of input vibration frequency for each device. The dimensions of the cantilevers, calculated output power density and other relevant parameters are listed in **Table 2**. Compared to PZT-5A and PZT-5H which were doped with ‘‘soft’’ (donor) dopants, KNBNNO contained oxygen vacancies equivalent to a ‘‘hard’’ (acceptor) doping effect, resulting in a larger quality factor for KNBNNO than those of PZT-5A and PZT-5H (Table 2).[36] Note that the parameters in Table 2 were optimized in the cantilevers to deliver relatively large outputs, and this is the reason that the output powers in Figure 2 are much larger than that in Figure 1(a). As shown in Figure 2 and Table 2, the KNBNNO was able to achieve roughly 20 % of the PZT’s performance. This was simply because the relevant piezoelectric parameters (Table 1) of the KNBNNO were significantly below those of the PZT family.[52] However, it should be pointed out that the purpose of this paper is to demonstrate the feasibility of using multi-functional materials to act as the sole component in a multi-source energy converter, and thus to inspire further development of the materials. It is clear that if the piezoelectric properties of multi-functional materials such as KNBNNO could be further improved, they could not only be individually competitive with the current widely used piezoelectrics but also possess the

additional benefit of being able to exhibit other energy conversion effects simultaneously. This aspect is discussed in the following sections.

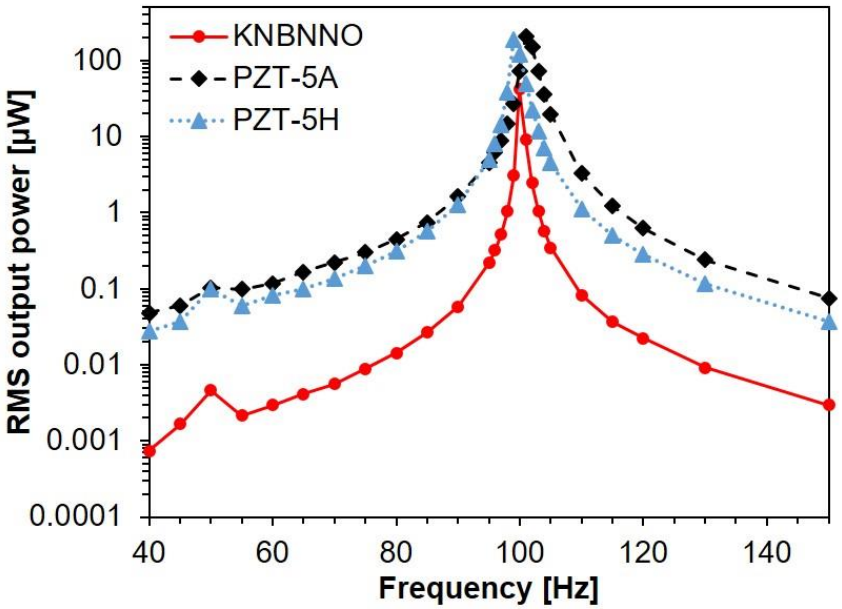

Figure 2. Dependence of piezoelectric output power (RMS) on input vibration frequency for cantilevers made of KNBNNO, PZT-5A and PZT-5H.

Table 2. Parameters associated with Figure 2.

	KNBNNO	PZT-5A	PZT-5H	Steel substrate
Length [mm]	9	9	9	29
Width [mm]	5.4	5.4	5.4	5.4
Thickness [μm]	202	195	237	150
Volume [mm^3]	9.82	9.48	11.52	
Length deducting the clamped part (free length) [m]	7.8	7.8	7.8	25.4
Capacitance [nF]	1.6	4.6	4.5	
Quality factor	139	46	57	
Resonant frequency [Hz]	100	101	99	
Acceleration [m s^{-2}]	4.9	4.9	4.9	
Maximum output power [μW]	41.4	208.9	185.9	
Maximum power density [mW cm^{-3}]	4.2	22.0	16.1	

2.2.2. Photovoltaic effect

In Figure 1(c), a typical DC (direct current) output generated via the photovoltaic effect appeared when the input light source was turned on. The output signal saturated within 5 seconds and then remained stable until the light source was turned off. It has been reported that the output signal of KNBNNO can remain stable for a long time.[37] This is the main practical advantage of using narrow band gap perovskite oxides as light absorbers and solar cells because the alternative, highly efficient organic-halide perovskite thin-film counterparts struggle with poor stability and their output decays rapidly within hours or days.[53] Similarly to the case of the piezoelectric output of this device, the output power density under the light source was also very small compared to value quoted for other solar cell counterparts. There were a couple of reasons responsible for the small output. Firstly, the spot size of the light source was only 0.5 mm^2 compared to the surface area (120 mm^2) of the KNBNNO, i.e. only 0.4 % of the surface area was subject to illumination. Secondly, the light source was a single-wavelength laser, whereas solar cell characteristics are typically measured under a solar simulator generating a spectrum very similar to the real solar spectrum and with a 100 mW cm^{-2} standard ‘‘one sun’’ illumination (AM 1.5G).[54] In this work, the multi-source measurement setup was restricted by space and a laser source was used instead. Although producing a lower power it still realized the purpose of the demonstration.

In previous works, the peak photovoltaic energy conversion efficiency (PEC) achieved for the KNBNNO under the same laser source was 0.12 %.[37] However, despite this PEC, the band gap of the KNBNNO was 1.6 eV (Table 1), comparable to a reported multi-junction BFCO ($BiFeCoO_3$) thin-film solar cell configuration which reached a PEC of 8.1 % measured under AM 1.5G illumination.[55] Meanwhile, considering the data reported in corresponding research into $BaTiO_3$ single crystals with a PEC of 4.8 % (AM 1.5G) but a wide band gap of > 3 eV,[56] the optimized PEC of the KNBNNO is expected to reach at least a few percent under standard AM 1.5G illumination with an optimized cell configuration (e.g. matched electrodes and charge

transporters, reduced thickness). This would be comparable to organic, thin-film and dye-sensitized TiO_2 counterparts.[54] A potentially effective method to improve the energy conversion efficiencies or capabilities of the piezoelectric and photovoltaic effects simultaneously would be to fabricate single crystals or highly oriented thin-films of KNBNNO.[57] In this work, the KNBNNO was a ceramic in which randomly oriented grains may hinder complete poling and thus suppress piezoelectricity, whilst the large number of grain boundaries may accelerate charger carrier recombination and hence degrade the PEC.[39, 57, 58]

2.2.3 Pyroelectric effect

In Figure 1(d), a typical pyroelectric response was also obtained. The temperature profile is shown in Figure 1(e). AC signals were generated with temperature change when turning the heat source on and off. In particular, the heat was turned on at the 10th second and the temperature started to increase (Figure 1(e)). As a response, pyroelectric current was generated from the harvester (Figure 1(d)). The heating process tended to degrade the ferroelectric domain alignment, thus changing the surface charge density of the KNBNNO element and inducing a pyro-current. Subsequently, the heat was turned off at the 28th second and the temperature started to decrease (Figure 1(e)). The cooling process tended to increase the alignment of the ferroelectric domain of the KNBNNO and again induced a pyro-current (Figure 1(d)). The same procedure was repeated in the 75th-90th seconds (Figure 1(d) and (e)). Note here that the heat on/off was controlled by the heat source (a heat gun) distant from the KNBNNO and the temperature was measured from the thermometer which was placed close to the KNBNNO (see the Experimental Section, Figure 7 and Figure 8 below). Therefore, there was a delay between the heat on/off and the inflexions of the temperature curve (Figure 1(e)). Furthermore, the pyro-current was extracted from the KNBNNO which corresponded to its real temperature change rather than the indicative temperature curve shown in Figure 1(e). Due to different heat capacities of the KNBNNO and the steel substrate (see the Experimental Section below),

heating of the materials was likely to be uneven and thus the real temperature change in the KNBNNO could fluctuate, leading to the changes in the pyro-current observed in Figure 1(d).

It is admitted that proper applications of sole pyroelectric energy harvesters in reality are less common than those of piezoelectric harvesters and solar cells due to the fact that a rapid temperature change is necessary in order to make the energy conversion process reasonably efficient.[2] However, as KNBNNO is an ABO_3-structured perovskite with ferroelectric phase(s) present, its pyroelectric effect occurs naturally together with its ferroelectricity and piezoelectricity, as in its counterparts of KNN, PZT, $BaTiO_3$, etc..[52, 59] Other researchers have made efforts to define favored and practical applications for pyroelectric energy harvesters such as harvesting waste heat from oscillating heat pipelines, human inhalation and exhalation, and the hot lubricating oil used in manufacturing industries.[2] In addition, the pyroelectric effect has been widely used in heat sensors.[60, 61] Therefore, the benefit of involving the pyroelectric effect in this work is mainly its potential multi-source harvesting-sensing integration in a single material/component.

2.3. Double input energy sources

2.3.1. Simultaneous operation of piezoelectric and photovoltaic effects

Figure 3 shows the output current density and power density measured with the same setup but with both vibration and light sources as the input. The cumulative effect on the peak output current density and power density of the sources can be clearly seen. When the vibration source only was turned on, the output performance was similar to that of Figure 1(a). When the light source was introduced whilst keeping the vibration on, the output behavior was equivalent to the sum of those of Figure 1(a) and (c). This add-on effect was also true when turning the light source on first and followed by the vibration, as shown in Figure 3. The smaller peak output current and power densities in Figure 3 when only the vibration source was present (i.e. approximately from the 5^{th} second to the 23^{rd} second) as compared to those of Figure 1(a), was

because the input frequency was slightly shifted away from the resonant frequency of the cantilever. It is well known that in a linear cantilever-structured piezoelectric energy harvester, the electric output is very sensitive to the frequency of the input vibration. Half of the peak output may be lost by shifting only < 5 % of the input frequency away from the resonant frequency.[30, 31] The resonant frequency of the fabricated device in this paper was about 15.3 Hz, according to the data shown in Figure 1(a). The measured frequency in Figure 3, however, was 15.7 Hz. Such a 3 % difference accounted for the output reduction.

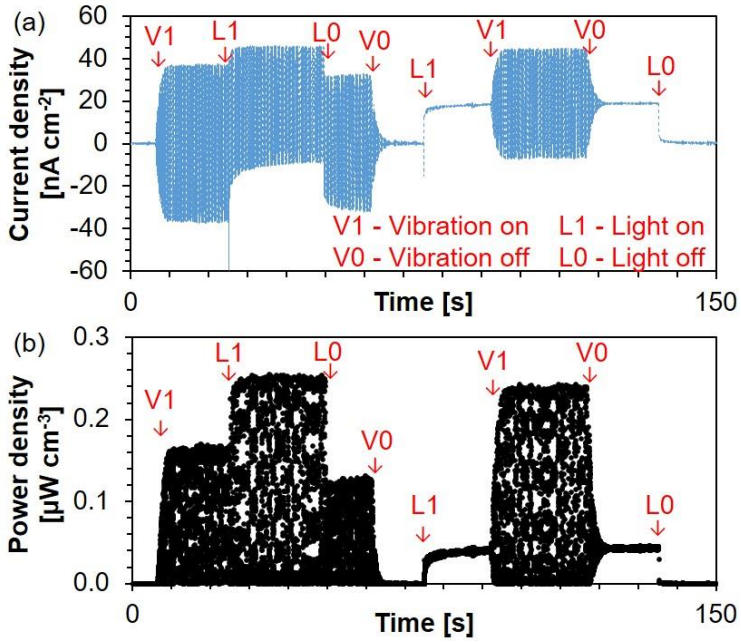

Figure 3. (a) Output current density and (b) output power density of the KNBNNO cantilever with vibration and light input energy sources.

On the other hand, in Figure 3(a) the photovoltaic current density was approximately 20 nA cm^{-2}, consistent with that shown in Figure 1(c). However, the peak-to-peak piezoelectric current density decreased from about 70 nA cm^{-2} when operating individually (i.e. 10^{th}-25^{th} second in Figure 3(a)) to 50 nA cm^{-2} when coupled with the photovoltaic effect (i.e. 30^{th}-50^{th} second and 95^{th}-120^{th} second in Figure 3(a)). It has been reported that illumination could change the permittivity and thus capacitance, as well as resistivity and thus resistance, of the KNBNNO.[62] The changed capacitance and resistance could alter the resonant frequency of the

KNBNNO element, leading to a reduced output current density (in the same way as presented above).[63] This is the reason that the add-on effect of the piezoelectric current density (35 nA cm^{-2} – positive maximum) and photovoltaic current density (20 nA cm^{-2}) did not fulfill the linear superposition (45 nA cm^{-2} in reality instead of 55 nA cm^{-2} in theory).

Figure 3 indicates three potential applications of the device. First, solar (visible light) and kinetic energy could be simultaneously harvested for electricity generation. Secondly, the device could be a double-source sensor, where the photovoltaic DC output and the piezoelectric AC output could be detected simultaneously with the help of advanced interface circuits and specially programed analyzing software. Finally, the photovoltaic effect could be used for harvesting energy with the DC output in order to self-power potential interface circuits to be built for use with the device. The piezoelectric effect could be used for sensing because the AC output can be distinguished from the DC output. Conversely, the piezoelectric effect could be used for energy harvesting and the photovoltaic effect for sensing. It should be noted that the utilization of the multi-functional, multi-source energy conversion material, KNBNNO, brings a significant novelty to the fabricated device and potential applications proposed above. All the multi-source harvesting, multi-functional sensing and harvesting-sensing functions could be realized with only a single material. This is considered to be a fundamental advance over the currently adopted solution of hybrid structures.[2, 32]

2.3.2. Effect of static strain on photovoltaic output

As previously reported, the performance of organic-halide perovskite thin-film solar cells degrades significantly when subject to external strain.[53] In order to understand the effect of strain on KNBNNO, different static strains were applied while the fabricated device was being measured under the light source. In static status (i.e. the vibration was off), the tip of the cantilever was bent upwards and downwards constantly by a micro-positioning stage. In this case, strain was transferred through the cantilever to the KNBNNO. The KNBNNO was thus

being compressed or stretched statically whilst the photovoltaic effect was operating. **Figure 4** shows the photocurrent densities of the fabricated device measured under the light source and with different static tip displacements, and their comparison with that of the free boundary condition.

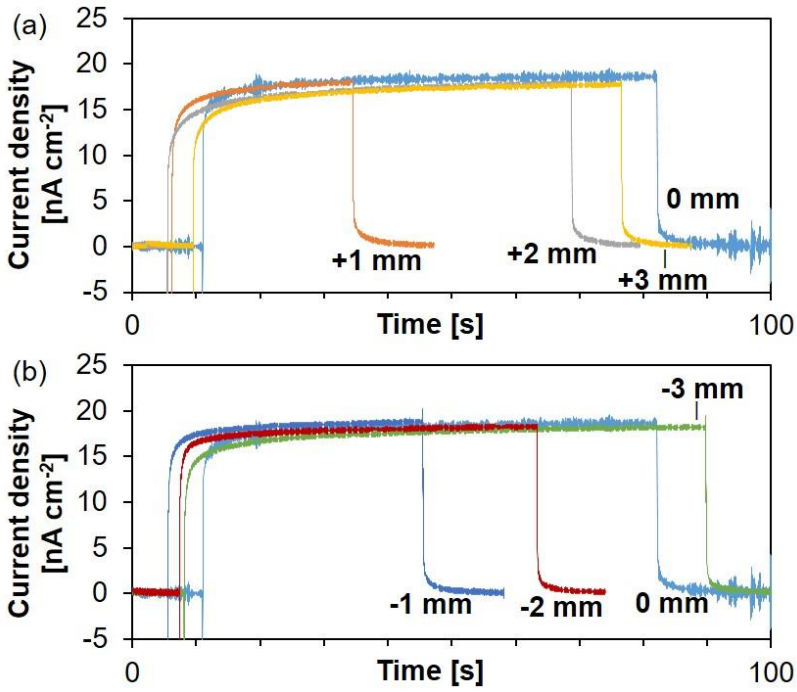

Figure 4. Current density of the fabricated device measured under the light source and with different constant tip displacements of the KNBNNO cantilever: (a) The cantilever tip bent upwards (with sign '+'), equivalent to the KNBNNO being subject to static compressive stress; (b) The cantilever tip bent downwards (with sign '-'), equivalent to the KNBNNO being subject to static tensile stress. The numbers represent the values of corresponding tip displacements. '0 mm' means the cantilever is under free boundary conditions, i.e. no tip displacement is applied.

A trend of a slight decrease of photocurrent density with increased externally introduced strain can be seen. In particular, when the tip displacement was increased from 1 mm to 3 mm, either upwards (Figure 4(a)) or downwards (Figure 4(b)), the photocurrent density showed a larger and larger decrease compared to that of 0 mm (no tip displacement). This could be

attributed to the interaction between incident light and domain wall motion, which has been comprehensively studied in previous works.[37, 62] It has been reported that incident light is able to stimulate the ferroelectric domain wall motion of KNBNNO.[37] It has also been suggested that domain walls may play an important role in photo-ferroelectric materials – i.e. ferroelectrics showing a photovoltaic effect.[64] Therefore, one could suggest that with 0 mm tip displacement and hence no external strain the interaction between incident light and domain wall motion was not interrupted. However, when strain was introduced, the domain wall motion was constrained.[58] Such a domain wall pinning effect might affect the photovoltaic output. It should be noted here that the working principles of ordinary semiconductor-based solar cells differ from those of photo-ferroelectrics such as KNBNNO. The latter are not fully understood and thus remain an open question.[64, 65] It can also be seen in Figure 4 that compression had a more obvious effect than tension, as the difference between the photocurrent densities of 0 mm and +3 mm (Figure 4(a), equivalent to compressive stress) was larger than that of 0 mm and -3 mm (Figure 4(b), equivalent to tensile stress). The exact influence of simultaneous strain and light on domain wall motion can be investigated via in-situ methods such as PFM (piezoresponse force microscopy). Such a research topic has not been well studied yet in the field. However, it should be stressed here that the results shown in Figure 4 experimentally prove that in this work the influence of strain on the photovoltaic effect for KNBNNO within the limit of the cantilever vibration amplitude was negligible. Therefore, the add-on effect of piezoelectric and photovoltaic energy conversions shown in Figure 3 is feasible.

Although the photocurrent density was affected by the introduced strain, the largest difference in photocurrent density noticed between 0 mm and +3 mm was less than 5 % while the difference between 0 mm and ±1 mm was not even noticeable. Considering that the peak-to-peak tip displacement of the cantilever was only 205 µm during the measurements, the degradation or interaction (if any) between the dynamic behavior and the photovoltaic effect was considered to be negligible. This also indicates that KNBNNO is more reliable and stable

than organic-halide thin-films for potential applications of solar-kinetic dual-source energy conversion.

2.3.3. Simultaneous operation of photovoltaic and pyroelectric effects

Figure 5(a) show the output of the fabricated device when subject to both light and heat energy sources. Figure 5(b) gives the temperature profile of the measurement. The response shown in Figure 5(a) indicated a very similar principle to that of Figure 3, except that the piezoelectric output was replaced by the pyroelectric output. A similar add-on effect between the DC and AC outputs generated by the photovoltaic effect under a light source and the pyroelectric effect under temperature fluctuation, respectively, could be observed. Incident light could cause localized heating and thus induce a pyroelectric effect, leading to erroneous photovoltaic observations. However, in this work the light source was a 405 nm laser which only induced a local temperature change of 0.5 °C in the KNBNNO.[37, 62] Such a change is negligible compared to the nearly 45 °C shown in Figure 5(b). Therefore, the photovoltaic effect observed in this work was true and was not induced by the pyroelectric effect. In Figure 5(a) the photovoltaic current density, 20 nA cm^{-2}, was consistent with that of Figure 1(c). In Figure 1(d) the maximum pyroelectric current density was about 40 nA cm^{-2}, while in Figure 5(a) the added on peak current density of the pyroelectric and photovoltaic effects was only 40 nA cm^{-2} instead of the estimated value of 60 nA cm^{-2}. The decreased pyroelectric influence on the overall current density was simply caused by a decreased temperature change (24-69 °C in Figure 5(b) compared to 24-75 °C in Figure 1(e)). Nevertheless, it has been proved in previous work that on KNBNNO the add-on effect of the pyroelectric and photovoltaic energy conversions fulfilled a perfect linear superposition with precisely controlled temperatures.[36]

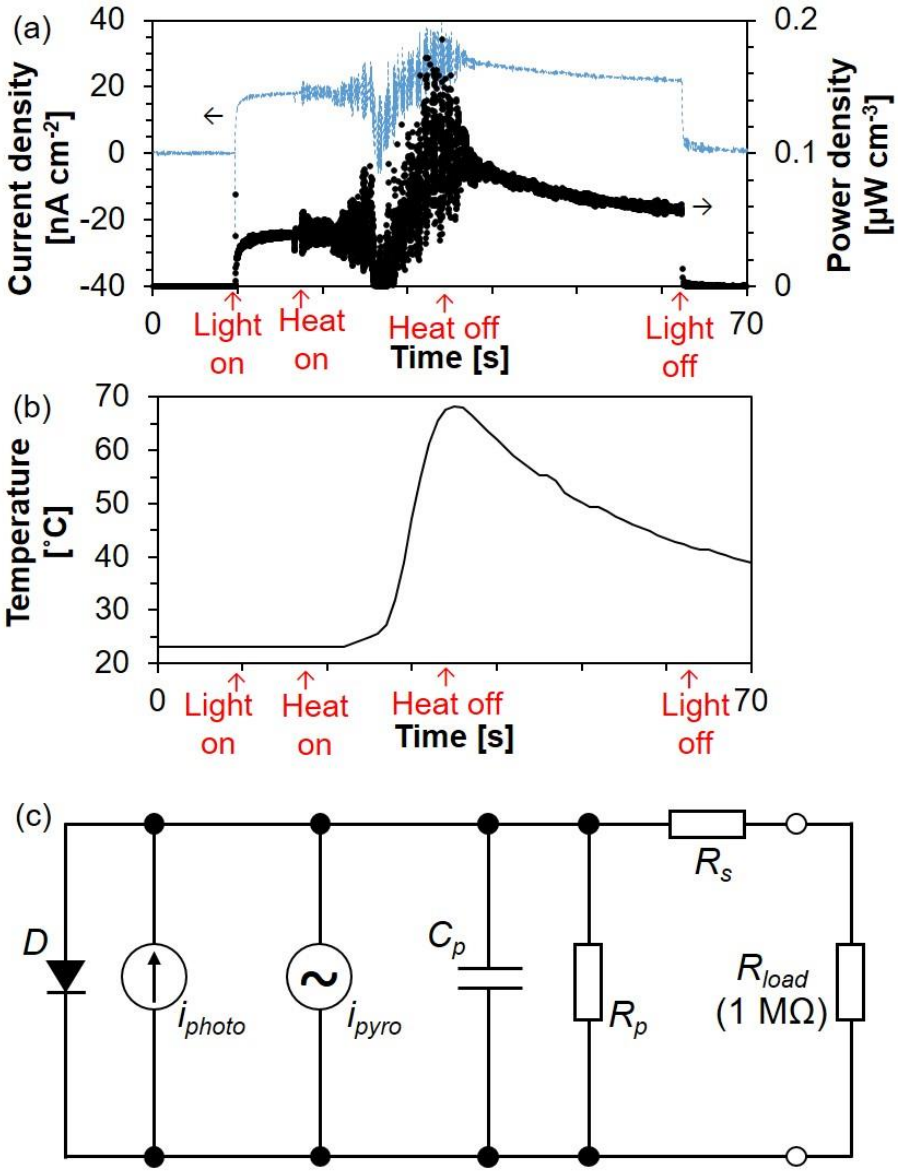

Figure 5. (a) Output current density and power density of the KNBNNO cantilever with light and heat input energy sources. (b) Temperature profile of the measurement shown in (a). (c) Equivalent circuit of the photovoltaic-pyroelectric coupling effect.

Equivalent circuits of piezoelectric, ferroelectric photovoltaic and pyroelectric energy converters have been reported in literature.[66-68] For multi-source energy harvesters which combine different individual piezoelectric, photovoltaic and pyroelectric components into one circuit platform, the equivalent circuit can be a simple parallel connection of the different components. However, the situation in this work was significantly different as the multiple output source came from a single material instead of three. Figure 5(c) shows a possible

example of the equivalent circuit of the photovoltaic-pyroelectric coupling in Figure 5(a). Both the photocurrent (i_{photo}) and the pyro-current (i_{pyro}) were generated in the KNBNNO, where the i_{photo} and i_{pyro} were DC and AC, respectively. The Schottky diode (D) came with i_{photo} for ferroelectric oxide solar cells.[68] C_p and R_p are the capacitance and parallel resistance of the KNBNNO, which may be affected by illumination and temperature.[37, 62] The series resistance (R_s) accounts for all the voltage drops from the current sources (i_{photo} and i_{pyro}) to the connection with the external resistive load (R_{load}).[68, 69]

Similarly, potential applications can be simultaneous double-source harvesting and sensing of solar (visible light) and thermal (temperature fluctuation) energy sources/stimuli, and harvesting using the photovoltaic effect for DC signals and sensing using the pyroelectric effect with distinguished AC signals (or *vice versa*). Counterpart concepts have also been reported, including (1) the use of simultaneous coupling of thermoelectric and photoelectric effects in a SnSe:Br semiconductor to convert temperature gradient into electricity via the thermoelectric effect whilst detecting photons via the photoelectric effect,[70] and (2) the use of carbon sponge material for simultaneous solar distillation and waste heat harvesting (to generate electricity).[71]

2.4. Justification of the AC-DC signal balance

It can also be noticed in Figure 3(a) and Figure 5 that the negative current in the AC signals opposed the positive DC signals. In practice, if no specifically designed rectifiers are used with the device, the negative part of the output current will tend to cancel the positive part, leading to decreased or even zero output power, although the positive parts will definitely show the add-on effect as mentioned above. This might not be a major issue if the device is to be used solely for sensing purposes but it has to be addressed if energy harvesting is to be the main purpose for such a device. This brings novel (though challenging) tasks to the design of

advanced circuitry. A rectification-free and/or energy harvester-storage integration design of the device may also help to solve the issue.[72-74]

Nevertheless, conventional diode bridge-type AC-DC converters can still be used for the rectification of harvested energy if a particular working environment for the device can be identified where solar, thermal and kinetic energy sources exist alternatively rather than simultaneously for the majority of the time.[75] For instance, recreational or well-being wearable electronics may satisfy such an energy scenario where the wearer goes to the gym for excise and also performs normal activities outdoors. It is known that piezoelectric energy harvesters work much better with a harmonic input vibration than with a random input of kinetic energy.[31] When the wearer does indoor exercise in the gym, there will be insufficient light (0.04 % of outdoor sunlight, mentioned above) for the wearable device equipped with the proposed multi-source energy harvester as described in this paper. However, the periodic excitation given to the harvester via running or aerobics will become the major effective energy source for the piezoelectric effect. The generated AC output is expected to be orders of magnitude larger than the DC output and thus can be rectified normally. When the wearer does normal activities outdoors, due to the random kinetic excitation, the piezoelectric AC output will become orders of magnitude smaller than the photovoltaic DC output under sufficient sunlight. By comparing the signals and then switching the power conditioning mode the issue of signal contradiction could be resolved.

In scenarios similar to those presented above, the trade-off between the DC and negative AC signals can be realized. In the meantime, the novelty of the device proposed in this paper over that of conventional hybrid energy harvesters (e.g. installation of both a solar cell and an individual piezoelectric harvester in the wearable device) is still valid because the space saving made by the single-material, multi-source harvester is crucial for miniaturizing designs of wearable electronics and other relevant wireless sensor networks.

2.5. Triple input energy sources

Figure 6(a) and (b) show the output current and power densities, respectively, of the fabricated device characterized with light, vibration and heat input energy sources. Again, the measured temperature data are plotted in Figure 6(c). The output behavior can be clearly seen as the combination of those shown in Figure 1. Most of the discussions about the add-on effect and trade-offs have been given above. It is noticed that when the heat was turned on, the output current showed a decrease and then a subsequent increase when the heat was turned off (Figure 6(a) and (c)). This is because the pyro-current had opposite directions when responding to a temperature increase and decrease,[67] and, the polarity depends on how the KNBNNO was connected. In the case of Figure 6, when the heat was turned on, the pyro-current was counteracting the net current (piezo-current + photocurrent) since the pyro-current direction was opposite to the net current direction, leading to a decrease of the overall output current. By the same principle, the temperature decrease when the heat was turned off induced a pyro-current in the same direction as the net current, resulting in an add-on effect of the net current (Figure 6(a) and (c)). The reason why the add-on effects of the piezoelectric, pyroelectric and photovoltaic energy conversions was not observed to be in a linear superposition has been explained separately in Sections 2.3.1 and 2.3.3.

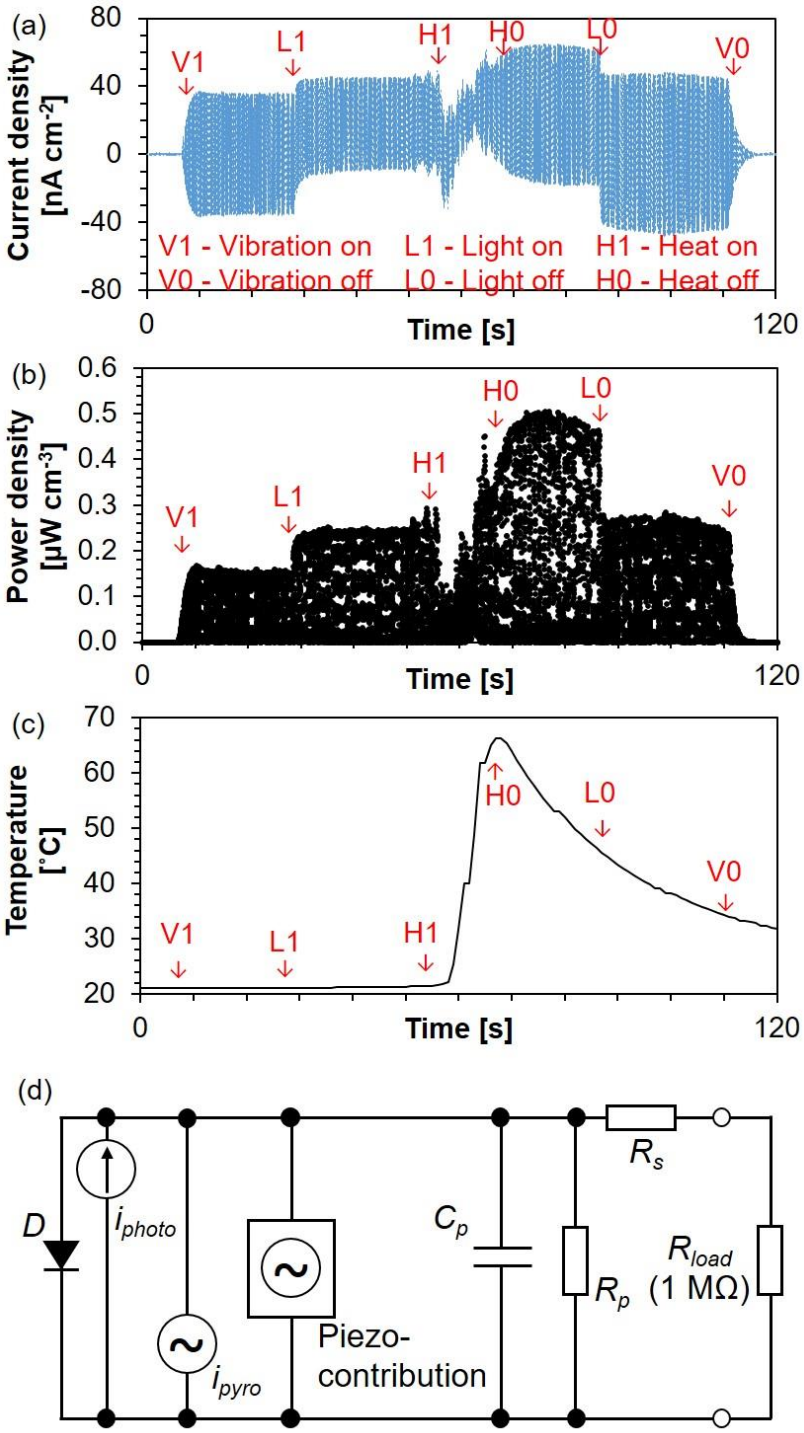

Figure 6. (a) Output current density and (b) output power density of the KNBNNO cantilever with vibration, light and heat input energy sources. (c) Temperature profile of the measurement shown in (a) and (b). (d) Equivalent circuit of the piezoelectric-photovoltaic-pyroelectric coupling effect.

The equivalent circuit of the piezoelectric-photovoltaic-pyroelectric coupling effect in the same material (KNBNNO), as shown in Figure 6(d), is more complex. Although the added on equivalent circuit for static photovoltaic and pyroelectric effects (Figure 5(c)) was relatively straightforward, the involvement of the dynamic piezoelectric effect brought in the electric equivalences of the mechanical parts, i.e. the mass, spring and damping factors.[66] These factors are determined by the active piezoelectric (KNBNNO) and inactive (steel, see Experimental Section) materials, the dimensions and configurations of the device, and, as presented above, they can be affected by illumination and temperature. They may also interact with the photovoltaic and pyroelectric current sources. Therefore, the complexity introduced by the piezoelectric effect is expressed as a black box in the equivalent circuit in Figure 6(d). The electric equivalences of the dynamics in the black box have been studied in literature.[66]

Potential applications of multi-source harvesting, multi-functional sensing and harvesting-sensing integration with a single material can be expected. With the analysis of the performance of simultaneous triple input energy sources, the ultimate purpose of the demonstration has been achieved and the scope of this paper fully revealed. The functional combination of harvesting and/or sensing of three different energy sources into the same material may contribute to a space saving of up to 67 % for the device design, as three different materials/components instead of one were necessary to realize the same multi-functionality prior to this work. The single-material but multi-functional feature of the ground-breaking material, KNBNNO, gives novelty to the fabricated harvesting-sensing device. The concept of using one material for multiple tasks proposed in the authors' previous works (either harvesting or sensing or both) is further elaborated here with a practical device responding to different energy sources equivalent to realistic conditions.[2, 57] The presented results are also expected to inspire further advances in relevant works in materials, systems and circuitry. For instance, the triple-source energy conversion in this work makes a leap in the single material device

design from previously reported dual-source counterparts like the use of ZnO for simultaneous piezoelectric and thermoelectric effects to harvest kinetic and thermal energy.[76]

3. Conclusion

Using a novel multi-source energy conversion material, KNBNNO, a single-material, multi-functional energy harvesting and/or sensing device has been fabricated and characterized. This device is the first of its kind in energy harvesting research, where solar, thermal and kinetic energy sources have been simultaneously harvested with a single energy conversion material/component. The previously proposed concept of using one material for multi-source energy conversion has been practically realized for the first time and has been further elaborated in this paper. The single-source and multi-source energy conversion behavior of the device, as well as its potential applications, the fundamental advantages of using such a device compared to conventional hybrid counterparts, and technical issues that need to be addressed for a more practical and feasible further development, have been discussed in detail. In particular, the effect of dynamic behavior on the photovoltaic effect has been assessed and discussed. The potential functions of the device are versatile, including multi-source energy harvesting, multi-stimuli sensing or harvesting-sensing integration with only one material/component. Such a single-material feature may make the commonly seen compromise of using multi-functionality to design miniaturization no longer necessary in relevant smart electronic devices and wireless sensors networks. This also contributes to the energy-efficient operation of those devices and sensors. At least 67 % space saving can be expected compared to those of conventional hybrid configurations.

4. Experimental Section

KNBNNO ceramic fabrication: Powder with the composition of $0.98(K_{0.5}Na_{0.5})NbO_3$-$0.02Ba(Ni_{0.5}Nb_{0.5})O_{3-\Delta}$ was prepared by solid state reaction. The starting reactants of K_2CO_3

(≥ 99 %, J. T. Baker, USA), Na_2CO_3 (≥ 99 %, Sigma-Aldrich, USA), $BaCO_3$ (99.98 %, Aldrich Chemistry, USA), NiO (99.999 %, Aldrich Chemistry, USA) and Nb_2O_5 (99.9 %, Aldrich Chemistry, USA) were weighed according to the stoichiometry. After mixing using a planetary ball mill (Pulverisette 6, Fritsch, Germany), the mixed powder was subject to a one-step calcination at 850 ˚C for 4 hours in air. The calcined powder was then ball-milled again and uniaxially pressed into green body discs with a 25 mm-diameter die. PVA (polyvinyl alcohol) was used as the binder. The subsequent binder burn-off and sintering were carried out at 500 ˚C for 10 hours and 1165 ˚C for 2 hours, respectively. The surfaces of the sintered samples were roughly polished with a P1200 silicon carbide abrasive paper (Eco-Wet, KWH Mirka Ltd., Finland).

Device fabrication: The sintered KNBNNO ceramic samples were laser-machined to obtain thin bulk samples. The machined surfaces were polished to reduce the surface roughness with the same P1200 silicon carbide abrasive paper mentioned above using ethanol as the coolant. Both surfaces of the samples were successively polished on a 3 µm grain-sized plate (MD Dur, Struers, Denmark) with diamond suspension (DiaPro Mol B3, Struers, Denmark), and on a 1 µm grain-sized plate (MD Nap, Struers, Denmark) with a finer diamond suspension (DiaPro Nap B1, Struers, Denmark). The final thickness was about 100 µm. One of the surfaces was coated with Ag paste (DT1402, Heraeus, Germany) by screen printing and fired at 600 ˚C for 20 minutes to form the back electrode. The other surface was further polished to a surface roughness of 5-10 nm using a 0.25 µm diamond suspension (DiaPro Nap ¼, Struers, Denmark). This surface was coated with 200 nm thick ITO (indium tin oxide) to form the transparent top electrode. The samples with their electrodes were then laser-cut to a rectangular shape (10 mm x 12 mm), and poled at room temperature in silicone oil with an electric field of 6 V μm^{-1}. Each rectangular sample was attached to a stainless steel beam (10 mm x 50 mm, thickness 100 µm) using Ag epoxy (Epo-Tek H20E, Epoxy Technology Inc., USA). A hole was drilled on the beam beforehand by laser for the purpose of being mounted on a shaker (presented

below). In this case, unimorph cantilevers were made and the stainless steel beam acted as the bottom electrode at the same time. Wires were connected to the ITO electrode and the beam, respectively. A mass of 1.4 g was attached to the tip of the beam. **Figure 7** shows the design and appearance of the fabricated device.

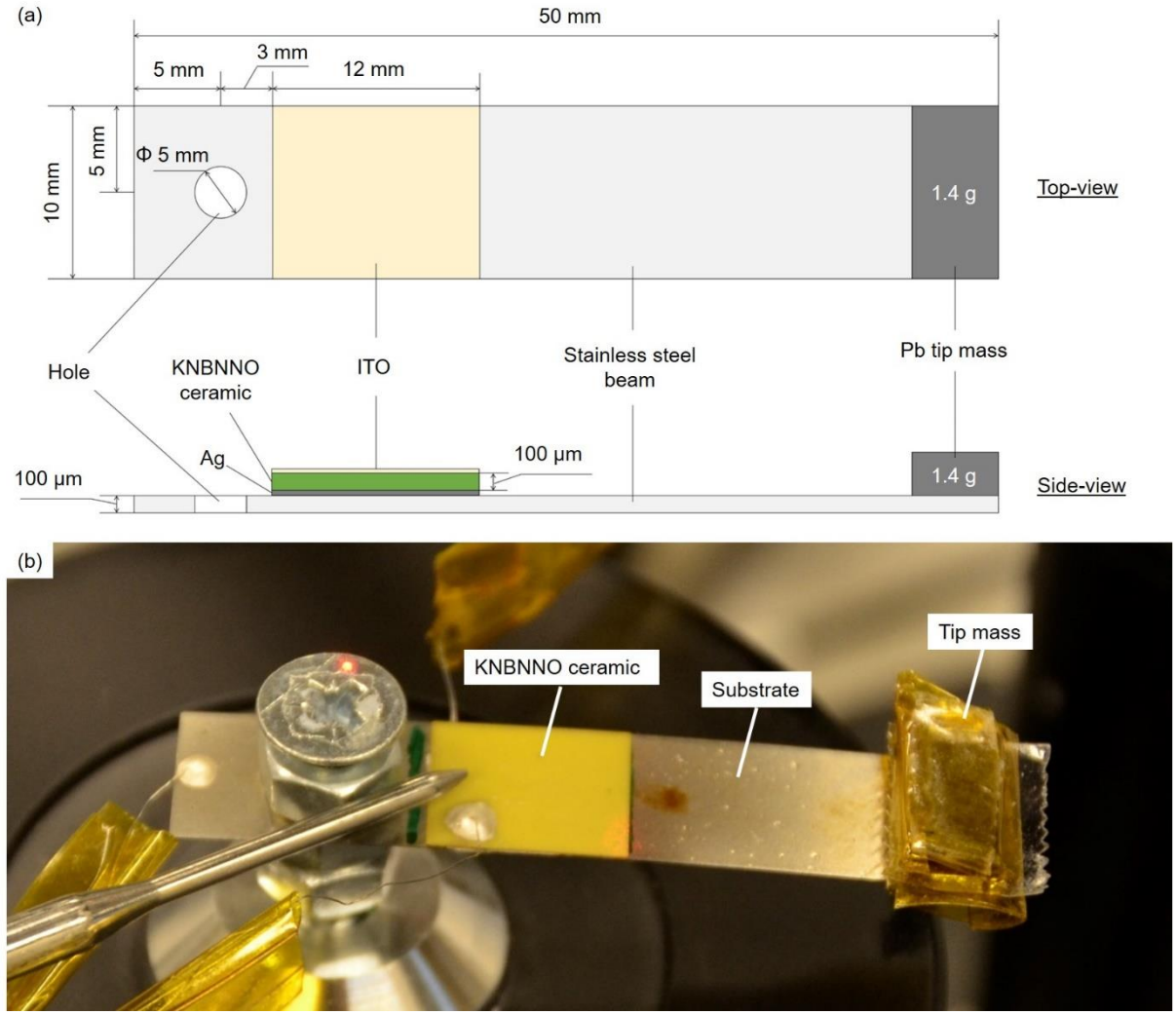

Figure 7. The (a) schematic and (b) picture of a fabricated energy harvesting-sensing device (KNBNNO cantilever).

Device characterization: The entire characterization system together with the multiple energy sources is shown in **Figure 8**. The cantilever was mounted by a screw on the shaker (Type 4810, Brüel & Kjær, Denmark) which provided the vibration (kinetic) energy source. The dynamic behavior (i.e. frequency and amplitude) of the shaker and the cantilever was

monitored by a laser interferometry system (OFV, Polytech, Germany). Another laser (OBIS, Laser System, Coherent, USA) with 405 nm wavelength, 50 mW output power and 0.5 mm^2 spot size provided the light source. The mirrors were set to reflect the laser beams onto the target positions. There were two beams from the interferometer. The reference beam was pointed at the base of the shaker (fixed part) and the measurement beam was pointed at the shaking part. The light source laser was pointed at the KNBNNO. The heat source was provided by a heat gun (RH 650V, Hitachi, Japan). The temperature near the KNBNNO was monitored by a thermometer. The two electrodes of the sample were connected with a 1 MΩ resistor and a high-precision electrometer (B2985A, Keysight, USA) in series. The current (I) of the entire circuit was measured by the electrometer. The output power (P) in the resistive load (R) was calculated by the equation $P = I^2 \bullet R$.

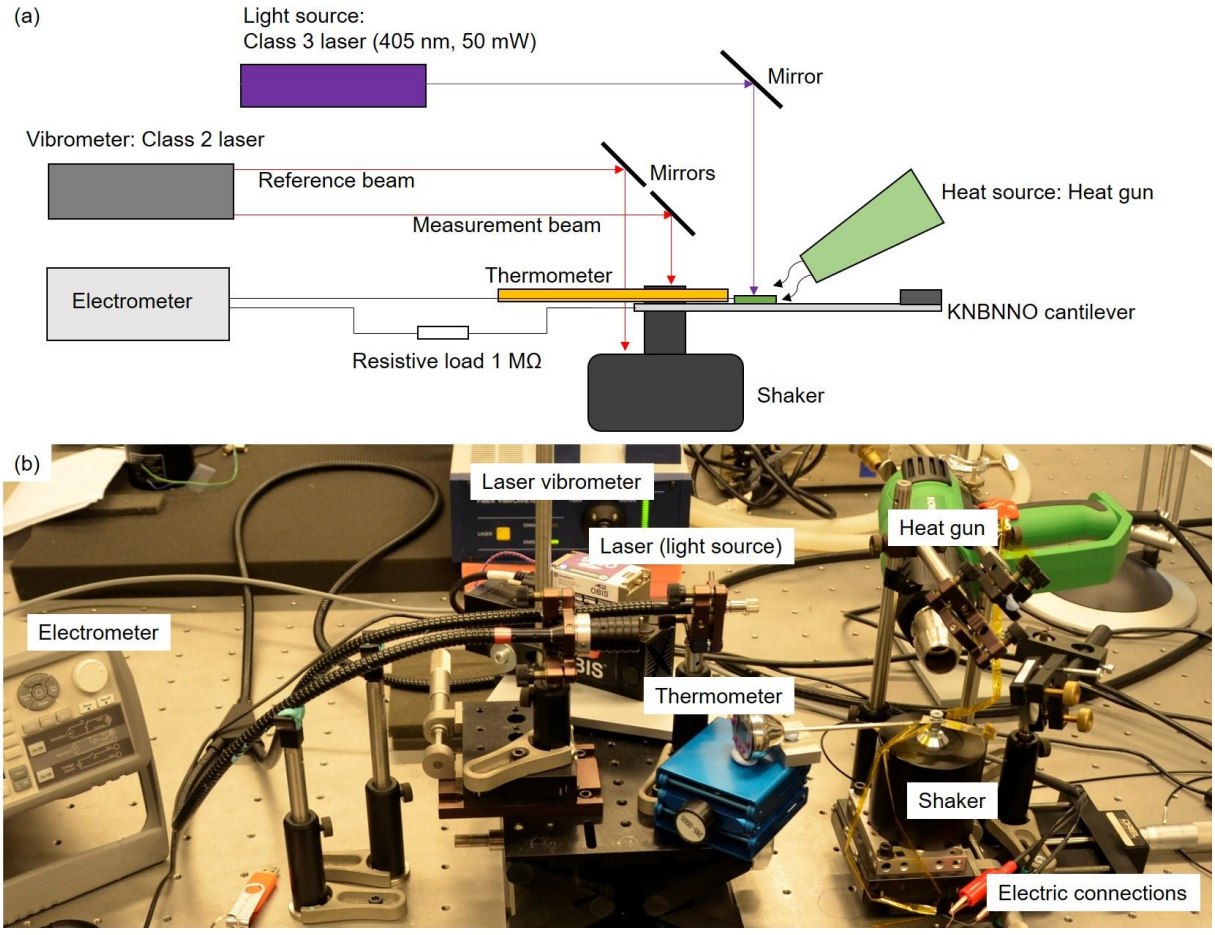

Figure 8. The (a) schematic and (b) picture of the multi-source characterization system.

Acknowledgements
Y.B. acknowledges the joint funding by the University of Oulu and Academy of Finland profiling action ‘‘Ubiquitous wireless sensor systems’’ (grant number 24302332). The authors also acknowledge the Centre for Material Analysis of the University of Oulu for the use of their facilities. P.T acknowledges the support of the Czech Science Foundation/GACR (projects No.18-20498S and No.17-08153S). Y.B. and J.P. fabricated the samples, carried out the characterizations and analyzed the data. P.T. helped to characterize the material properties. All authors co-wrote the paper and discussed the implications of the results.

Conflict of interest
The results reported in this paper are under the process of a patent application (application number FI20196042).

Received: ((will be filled in by the editorial staff))
Revised: ((will be filled in by the editorial staff))
Published online: ((will be filled in by the editorial staff))

References
[1] International Energy Agency, *Renewables 2018 - Market analysis and forecast from 2018 to 2023*, **2018**.
[2] Y. Bai, H. Jantunen, J. Juuti, *Adv Mater.* **2018**, *30*, 1707271.
[3] oulu.fi/6gflagship, accessed on 6/26 **2018**.
[4] EnOcean, *The true cost of batteries - why energy harvesting is the best power solution for wireless sensors*, **2015**.
[5] W. Liu, J. Chen, Z. Chen, K. Liu, G. Zhou, Y. Sun, M. Song, Z. Bao, Y. Cui, *Adv. Energy Mater.* **2017**, *7*, 1701076.
[6] K. Liu, B. Kong, W. Liu, Y. Sun, M. Song, J. Chen, Y. Liu, D. Lin, A. Pei, Y. Cui, *Joule* **2018**, *2*, 1857-1865.
[7] J. Wan, J. Xie, X. Kong, Z. Liu, K. Liu, F. Shi, A. Pei, H. Chen, W. Chen, J. Chen, X. Zhang, L. Zong, J. Wang, L. Chen, J. Qin, Y. Cui, *Nat. Nanotechnol.* **2019**, *14*, 705.
[8] S. Xu, X. Liang, X. Wu, S. Zhao, J. Chen, K. Wang, J. Chen, *Nat. Commun.* **2019**, *10*, 5810.
[9] G. Zan, T. Wu, P. Hu, Y. Zhou, S. Zhao, S. Xu, J. Chen, Y. Cui, Q. Wu, *Energy Storage Materials.* **2020**, *28*, 82-90.
[10] O. Kanoun, *Energy harvesting for wireless sensor networks*, De Gruyter, Berlin/Boston **2019**.
[11] O. B. Akan, O. Cetinkaya, C. Koca, M. Ozger, *IEEE Internet Things J.* **2018**, *5*, 736-746.
[12] N. Zhang, C. Tao, X. Fan, J. Chen, *J. Mater. Res.* **2017**, *32*, 1628-1646.
[13] K. Meng, S. Zhao, Y. Zhou, Y. Wu, S. Zhang, Q. He, X. Wang, Z. Zhou, W. Fan, X. Tan, J. Yang, J. Chen, *Matter.* **2020**, *2*, 896-907.
[14] Z. Zhou, S. Padgett, Z. Cai, G. Conta, Y. Wu, Q. He, S. Zhang, C. Sun, J. Liu, E. Fan, K. Meng, Z. Lin, C. Uy, J. Yang, J. Chen, *Biosens. Bioelectron.* **2020**, *155*, 112064.
[15] Y. Su, T. Yang, X. Zhao, Z. Cai, G. Chen, M. Yao, K. Chen, M. Bick, J. Wang, S. Li, G. Xie, H. Tai, X. Du, Y. Jiang, J. Chen, *Nano Energy.* **2020**, *74*, 104941.
[16] Y. Su, J. Wang, B. Wang, T. Yang, B. Yang, G. Xie, Y. Zhou, S. Zhang, H. Tai, Z. Cai, G. Chen, Y. Jiang, L. Chen, J. Chen, *ACS Nano.* **2020**, *14*, 6067-6075.
[17] K. Meng, J. Chen, X. Li, Y. Wu, W. Fan, Z. Zhou, Q. He, X. Wang, X. Fan, Y. Zhang, J. Yang, Z. L. Wang, *Adv. Funct. Mater.* **2019**, *29*, 1806388.

[18] J. Chen, Y. Huang, N. Zhang, H. Zou, R. Liu, C. Tao, X. Fan, Z. L. Wang, , *Nat. Energy.* **2016**, *1*, 16138.
[19] G. Chen, Y. Li, M. Bick, J. Chen, *Chem. Rev.* **2020**, *120*, 3668-3720.
[20] N. Zhang, F. Huang, S. Zhao, X. Lv, Y. Zhou, S. Xiang, S. Xu, Y. Li, G. Chen, C. Tao, Y. Nie, J. Chen, X. Fan, *Matter.* **2020**, *2*, 1260-1269.
[21] J. Chen, Z. L. Wang, *Joule* **2017**, *1*, 480-521.
[22] C. Yan, Y. Gao, S. Zhao, S. Zhang, Y. Zhou, W. Deng, Z. Li, G. Jiang, L. Jin, G. Tian, T. Yang, X. Chu, D. Xiong, Z. Wang, Y. Li, W. Yang, J. Chen, *Nano Energy.* **2020**, *67*, 104235.
[23] N. Zhang, J. Chen, Y. Huang, W. Guo, J. Yang, J. Du, X. Fan, C. Tao, *Adv Mater.* **2016**, *28*, 263-269.
[24] L. Jin, J. Chen, B. Zhang, W. Deng, L. Zhang, H. Zhang, X. Huang, M. Zhu, W. Yang, Z. L. Wang, *ACS Nano.* **2016**, *10*, 7874-7881.
[25] B. Zhang, J. Chen, L. Jin, W. Deng, L. Zhang, H. Zhang, M. Zhu, W. Yang, Z. L. Wang, *ACS Nano.* **2016**, *10*, 6241-6247.
[26] J. Chen, G. Zhu, W. Yang, Q. Jing, P. Bai, Y. Yang, T. Hou, Z. L. Wang, *Adv Mater.* **2013**, *25*, 6094-6099.
[27] S. Pu, Y. Liao, K. Chen, J. Fu, S. Zhang, L. Ge, G. Conta, S. Bouzarif, T. Cheng, X. Hu, K. Liu, J. Chen, *Nano Lett.* **2020**, *20*, 3791-3797.
[28] S. Pu, J. Fu, Y. Liao, L. Ge, Y. Zhou, S. Zhang, S. Zhao, X. Liu, X. Hu, K. Liu, J. Chen, *Adv Mater.* **2020**, *32*, 1907307.
[29] S. Roundy, P. Wright, J. Rabaey, *Comput. Commun.* **2003**, *26*, 1131-1144.
[30] Y. Bai, C. Meggs, T. W. Button, *Int. J. Struct. Stab. Dyn.* **2014**, *14*, 1440016.
[31] Y. Bai, P. Tofel, Z. Hadas, J. Smilek, P. Losak, P. Skarvada, R. Macku, *Mech. Syst. Signal Proc.* **2018**, *106*, 303-318.
[32] Y. Bai, H. Jantunen, J. Juuti, *Front. Mater.* **2018**, *5*, 65.
[33] Frost & Sullivan, *Technology impact assessment of micro energy harvesting*, **2018**.
[34] P. Cahill, N. Jackson, A. Mathewson, V. Pakrashi, *Damage Assessment of Structures X*, *Pts 1 and 2.* **2013**, *569-570*, 335-341.
[35] P. Cahill, V. Pakrashi, P. Sun, A. Mathewson, S. Nagarajaiah, *Smart. Struct. Syst.* **2018**, *21*, 287-303.
[36] Y. Bai, P. Tofel, J. Palosaari, H. Jantunen, J. Juuti, *Adv Mater.* **2017**, *29*, 1700767.
[37] Y. Bai, G. Vats, J. Seidel, H. Jantunen, J. Juuti, *Adv Mater.* **2018**, *30*, 1803821.
[38] Y. Bai, H. Xiang, H. Jantunen, J. Juuti, *Eur. Phys. J. -Spec. Top.* **2019**, *228*, 1555-1573.
[39] T. Zheng, J. Wu, D. Xiao, J. Zhu, *Prog. Mater. Sci.* **2018**, *98*, 552-624.
[40] Y. Bai, *PhD Thesis*, University of Birmingham **2015**.
[41] M. Stewart, P. M. Weaver, M. Cain, *Appl. Phys. Lett.* **2012**, *100*, 073901.
[42] J. Palosaari, M. Leinonen, J. Juuti, H. Jantunen, *Mech. Syst. Signal Proc.* **2018**, *106*, 114-118.
[43] Y. Liu, T. Yang, F. Shu, *Funct. Mater. Lett.* **2016**, *9*, 1650069.
[44] Y. Bai, Z. Havranek, P. Tofel, C. Meggs, H. Hughes, T. W. Button, *Eur. Phys. J. -Spec. Top.* **2015**, *224*, 2675-2685.
[45] T. Yildirim, M. H. Ghayesh, W. Li, G. Alici, *Renew. Sust. Energ. Rev.* **2017**, *71*, 435-449.
[46] L. Tang, Y. Yang, *Appl. Phys. Lett.* **2012**, *101*, 094102.
[47] I. Kanno, T. Ichida, K. Adachi, H. Kotera, K. Shibata, T. Mishima, *Sens. Actuator A-Phys.* **2012**, *179*, 132-136.
[48] J. H. Kim, J. S. Kim, S. H. Han, H. -. Kang, H. -. Lee, C. I. Cheon, *Ceram. Int.* **2016**, *42*, 5226-5230.
[49] V. Shah, R. Kumar, M. Talha, R. Vaish, *Integrated Ferroelectr.* **2016**, *176*, 73-84.
[50] M. Zheng, Y. Hou, L. Chao, M. Zhu, *J. Mater. Sci. -Mater. Electron.* **2018**, *29*, 9582-9587.
[51] Piezo.com, accessed on 4/10 **2020**.
[52] C. R. Bowen, H. A. Kim, P. M. Weaver, S. Dunn, *Energy Environ. Sci.* **2014**, *7*, 25-44.

[53] M. I. Asghar, J. Zhang, H. Wang, P. D. Lund, *Renew. Sust. Energ. Rev.* **2017**, *77*, 131-146.
[54] A. Polman, M. Knight, E. C. Garnett, B. Ehrler, W. C. Sinke, *Science.* **2016**, *352*, 4424.
[55] R. Nechache, C. Harnagea, S. Li, L. Cardenas, W. Huang, J. Chakrabartty, F. Rosei, *Nat. Photonics.* **2015**, *9*, 61-67.
[56] J. E. Spanier, V. M. Fridkin, A. M. Rappe, A. R. Akbashev, A. Polemi, Y. Qi, Z. Gu, S. M. Young, C. J. Hawley, D. Imbrenda, G. Xiao, A. L. Bennett-Jackson, C. L. Johnson, *Nat. Photonics.* **2016**, *10*, 688-688.
[57] Y. Bai, H. Jantunen, J. Juuti, *ChemSusChem.* **2019**, *12*, 2540-2549.
[58] D. Damjanovic, *Rep. Prog. Phys.* **1998**, *61*, 1267-1324.
[59] A. Chauhan, S. Patel, G. Vats, R. Vaish, *Energy Technol.* **2014**, *2*, 205-209.
[60] R. Whatmore, *Rep. Prog. Phys.* **1986**, *49*, 1335-1386.
[61] S. Lang, *Phys Today.* **2005**, *58*, 31-36.
[62] G. Vats, Y. Bai, D. Zhang, J. Juuti, J. Seidel, *Adv. Opt. Mater.* **2019**, *7*, 1800858.
[63] J. Palosaari, M. Leinonen, J. Hannu, J. Juuti, H. Jantunen, *J. Electroceram.* **2012**, *28*, 214-219.
[64] C. Paillard, X. Bai, I. C. Infante, M. Guennou, G. Geneste, M. Alexe, J. Kreisel, B. Dkhil, *Adv Mater.* **2016**, *28*, 5153-5168.
[65] P. Lopez-Varo, L. Bertoluzzi, J. Bisquert, M. Alexe, M. Coll, J. Huang, J. Antonio Jimenez-Tejada, T. Kirchartz, R. Nechache, F. Rosei, Y. Yuan, *Phys. Rep. -Rev. Sec. Phys. Lett.* **2016**, *653*, 1-40.
[66] B. Richter, J. Twiefel, J. Wallaschek, in *Energy Harvesting Technologies* (Eds: S. Priya, D. J. Inman), Springer, Boston **2009**, Ch. 4.
[67] C. R. Bowen, J. Taylor, E. LeBoulbar, D. Zabek, A. Chauhan, R. Vaish, *Energy Environ. Sci.* **2014**, *7*, 3836-3856.
[68] Z. Tan, L. Hong, Z. Fan, J. Tian, L. Zhang, Y. Jiang, Z. Hou, D. Chen, M. Qin, M. Zeng, J. Gao, X. Lu, G. Zhou, X. Gao, J. Liu, *NPG Asia Mater.* **2019**, *11*, 20.
[69] P. Würfel, U. Würfel, *Physics of solar cells: from basic principles to advanced concepts (Third edition)*, Wiley-VCH, Weinheim **2016**.
[70] B. Ouyang, C. Chang, L. Zhao, Z. L. Wang, Y. Yang, *Nano Energy.* **2019**, *66*, 104111.
[71] L. Zhu, M. Gao, C. K. N. Peh, X. Wang, G. W. Ho, *Adv. Energy Mater.* **2018**, *8*, 1702149.
[72] X. Xue, S. Wang, W. Guo, Y. Zhang, Z. L. Wang, *Nano Lett.* **2012**, *12*, 5048-5054.
[73] R. Song, H. Jin, X. Li, L. Fei, Y. Zhao, H. Huang, H. L. Chan, Y. Wang, Y. Chai, *J. Mater. Chem. A.* **2015**, *3*, 14963-14970.
[74] A. Ramadoss, B. Saravanakumar, S. W. Lee, Y. Kim, S. J. Kim, Z. L. Wang, *ACS Nano.* **2015**, *9*, 4337-4345.
[75] Y. Li, Z. Tang, Z. Zhu, Y. Yang, *Analog Integr. Cir. Signal Proc.* **2018**, *94*, 105-115.
[76] Z. Jin, J. S. Yang, *J Electron Mater.* **2018**, *47*, 4533-4538.